Energy Equip. Sys./ Vol. 6/No. 3/Sep. 2018/ 261-277

ENERGY EQUIPSYS

Energy Equipment and Systems

http://energyequipsys.ut.ac.ir
www.energyequipsys.com

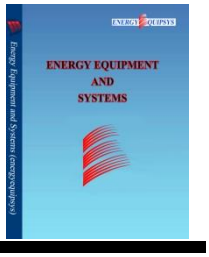

Combined mixed convection and radiation simulation of inclined lid driven cavity

Author

Maryam Moein Addini [a]
Abdolreza Gandjalikhan Nassab [a*]

[a] Department of Mechanical Engineering, School of Engineering, Shahid Bahonar University of Kerman, Kerman, Iran

Article history:

Received : 4 June 2017
Accepted : 4 April 2018

ABSTRACT

This paper presents a numerical investigation of the laminar mixed convection flow of a radiating gas in an inclined lid-driven cavity. The fluid is treated as a gray, absorbing, emitting, and scattering medium. The governing differential equations including continuity, momentum and energy are solved numerically by the computational fluid dynamics techniques (CFD) to obtain the velocity and temperature fields. The discretized forms of these equations are obtained by the finite volume method and solved by using the SIMPLE algorithm. Since the gas is considered as a radiating medium, besides convection and conduction heat transfer, radiation also takes place in the gas flow. For computing the radiative term in the gas energy equation, the radiative transfer equation (RTE) is solved numerically by the discrete ordinate method (DOM). The streamline and isotherm plots and the distributions of convective, radiative and total Nusselt numbers along the bottom wall of the cavity are presented. In this work, an attempt is made to investigate the hydrodynamic and thermal behavior of the mixed convection flow of a radiating gas at different values of the cavity inclination angle. The numerical results reveal that the variation of inclination angle causes a sweep behavior in the flow pattern inside the cavity. Besides, it is found that the value of radiative Nusselt number along the heated wall has a decreasing trend when the medium optical thickness is increases. Comparisons between the present numerical results with those obtained by other investigators in the cases of conduction-radiation and pure convection systems show good consistencies.

Keywords: Laminar Mixed Convection Flow, Lid-Driven Cavity, Inclination Angle, Radiation, DOM.

1. Introduction

Driven cavity flow has received considerable attention over the past 50 years, starting with the early work of Burggraf [1] for a square cavity. The lid-driven cavity is probably one of the most studied fluid problems in the area of computational fluid dynamics. Driven cavity flow serves as a benchmark problem to validate numerical solution algorithms [2]. Mixed convection flow occurs in lid-driven cavities due to both the shear force caused by the movement of the cavity wall and the buoyancy force produced by thermal non-homogeneity of the cavity boundaries. The problem of laminar mixed convection with lid-driven flows has multiple applications in the

[*] Corresponding author: Abdolreza Gandjalikhan Nassab
Department of Mechanical Engineering, School of Engineering, Shahid Bahonar University of Kerman, Kerman, Iran
Email: ganj110@uk.ac.ir

field of thermal engineering. The flow configuration is relevant to a number of industrial applications such as in food processing and float glass production [3], solar collectors [4], lake and reservoirs [5], nuclear reactors, solar ponds, and crystal growth phenomena [6].

In the mixed convection mode of heat transfer, the features of both forced and natural convections are important.

When analyzing potentially mixed convection, a parameter called the Richardson number ($Ri = Gr/Re^2$) denotes the relative strength of free and forced convections. In the case of $Ri >> 1$, natural convection becomes the main mechanism of heat transfer and when $Ri << 1$, forced convection dominates, and for $Ri = 1$, mixed convection takes place.

Numerical studies on lid-driven cavity flow and heat transfer involving different cavity configurations, various fluids and imposed temperature gradients have been published in the literature. Prasad and Koseff [7] reported experimental results of a mixed convection heat transfer process in a lid-driven cavity for a different Richardson number ranging from 0.1 to 1000. Heat transfer results for mixed convection from a bottom heated open cavity subjected to an external flow studied for a wide range of the governing parameters ($1 \leq Re \leq 2000$, $0 \leq Gr \leq 10^6$) over cavities with various aspect ratios (A = 0.5, 1, 2 and 4) were reported by Leong et al. [8]. The numerical simulations by Moallemi and Jang [9] focused on the two-dimensional laminar flow for a wide range of Reynolds numbers ($100 \leq Re \leq 2200$), and small-to-moderate Prandtl number ($0.01 \leq Pr \leq 50$) in a cavity for different levels of the Richardson numbers. It was found that the influence of buoyancy on the flow and heat transfer becomes important for higher values of Pr, if Re and Gr are kept constant. Oztop et al. [10] studied mixed convection in a lid-driven cavity with the presence of heaters at the corners. They observed that lid-direction was the most effective parameter of heat transfer from heaters.

The modeling and simulation of many studies for lid-driven cavity flow is generally grouped into the horizontal or vertical side wall sliding lid-driven cavity problems, except that the horizontal or vertical walls are differentially heated. In all the studies mentioned above, it was assumed that the gravitational field was aligned with geo-potential lines. In some engineering applications, however, the surface of the devices is rarely aligned with geo-potential lines. Moreover, depending on the direction, the inclined lid-driven cavity may aid or oppose buoyancy. As a result, fluid flow and heat transfer in an inclined cavity are different from those in a horizontal configuration. Therefore, the effect of inclination angle on the characteristics of heat transfer in a cavity is worthwhile for study. Sharif [11] examined laminar mixed convective heat transfer in a two-dimensional shallow inclined rectangular cavity. He found that the average Nusselt number increased slowly with cavity inclination for the forced convection dominated case, while it increased more rapidly with the inclination angle for the natural convection dominated case. Alinia et al. [12] conducted a numerical study on mixed convection in an inclined cavity. They found that the effect of inclination angle was more pronounced at high Richardson numbers due to the domination of natural convection. Oztop [13] worked on natural convection in partially cooled and inclined porous rectangular enclosures. Sivasankaran et al. [14] studied mixed convection in an inclined lid-driven cavity with different sizes and locations of the heater. They found that high heat transfer occurred at an inclination angle of 30° in the buoyancy convection dominated regime when the heater was located in the middle of the cavity. Mohammad and Viskanta [15] experimentally and numerically studied mixed convection in shallow rectangular bottom heated cavities filled with liquid Gallium having a low Prandtl number of 0.022. They found that the heat transfer rate was rather insensitive to the lid velocity and an extremely thin shear layer existed along the major portion of the moving lid. The flow structure consisted of an elongated secondary circulation that occupied a third of the cavity.

In studies focusing on mixed convection [16–19], the radiative mode of heat transfer is sometimes neglected because it requires an overwhelming amount of computational resources. Some studies in the literature try to show that radiation heat transfer has an important and significant effect on the system and cannot be neglected [20, 21]. In all the studies mentioned above, the effect of radiation heat transfer was neglected in the analysis, so that the gas energy equation only contained the convection and conduction terms. However, the radiation effect may be important even for

small temperature differences. Based on the author's knowledge, laminar mixed convection flow of a radiating gas in an inclined cavity has still not been studied theoretically or experimentally. Thereby, the present work deals with the numerical solutions of the continuity, momentum and energy equations for a radiating mixed convection gas flow in an inclined square lid-driven cavity by the CFD techniques. For computing the distribution of radiative heat flux, the RTE is solved numerically by the DOM. Finally, an attempt is made to investigate the effects of radiative parameters and inclined angle and also the Richardson number on the flow and heat transfer characteristics with an emphasis on the cavity inclined angle effect.

Nomenclature

A_x, A_y	areas of control volume faces normal to the x- and y-directions, respectively (m^2)
C_p	specific heat (J/kgK)
g	gravitational acceleration (ms^{-2})
Gr	Grashof number
h	heat transfer coefficient($Wm^{-2}K^{-1}$)
I	radiation intensity (W/m^2)
I^*	dimensionless radiation intensity
I_b	black body radiation intensity(W/m^2)
k	thermal conductivity($Wm^{-1}K^{-1}$)
L	cavity depth or width (m)
Nu_c	convective Nusselt number
Nu_r	radiative Nusselt number
(u,v)	horizontal and vertical velocity components (ms^{-1})
(U,V)	dimensionless horizontal and vertical velocity Components
U_0	lid velocity (ms^{-1})
w	quadrature weight associated within any direction $\boldsymbol{s}$
X, Y	dimensionless horizontal and vertical coordinates, respectively

Greek Symbols

α	thermal diffusivity (m^2/s)
β	extinction coefficient (m^{-1})
φ	phase function
ϕ	inclination angle
Ω	solid angle
σ	Stefan–Boltzmann constant, 5.67×10^{-8} W/m^2K^4
Nu_t	total Nusselt number
n_w	outward unit vector normal to the surface
p	pressure (Nm^{-2})
P	dimensionless pressure
Pr	Prandtl number, υ/α
q_c	convective heat flux
q_r	radiative heat flux
q^*	dimensionless heat flux
r	position vector (m)
RC	radiation-conduction parameter
Re	Reynolds number
Ri	Richardson number
S	radiation source function (W/m^2)
S^*	dimensionless radiation source function
s	geometric path vector
T	temperature (K)
σ_a	absorption coefficient (m^{-1})
σ_s	scattering coefficient (m^{-1})
ε	emissivity coefficient
μ	dynamic viscosity ($N.s/m^2$)
υ	kinematic viscosity (m^2/s)
ω	albedo coefficient
ρ	density (kg/m^3)
τ	optical thickness
Θ	dimensionless temperature
θ_1, θ_2	dimensionless temperature parameters

Subscripts

c	convective
r	radiative
h	hot
c	cold
w	wall

2. Theory

Two-dimensional laminar mixed convection of gas flow in an inclined lid-driven cavity by considering the gas radiation effect is numerically simulated. A schematic representation of the computational domain is

shown in Fig. 1. It consists of a square cavity of dimension L. The vertical and bottom walls are maintained at a uniform constant temperature. The top wall is considered as cold and the other walls are hot, while the top wall moves at a constant speed. During this study, the Reynolds number was fixed at 100 so that the Richardson number changed with the Grashof number. All the physical properties of the system are assumed to be constant, except for the density. The participating medium is assumed to be gray, and the emissivities of the walls are also assumed to be constant.

With this geometry and boundary conditions, the present study reports the computations for cavities at inclination angles ranging from 0° to 90°, and their effects on the heat transfer process is analyzed. The results are presented in terms of the streamline and isotherm plots in the cavity and the variations of convective and radiative Nusselt numbers at the bottom wall.

2.1. Basic Equation

For incompressible, steady, and two-dimensional laminar and constant property flow by assuming the Boussinesq approximation, the governing differential equations are the conservations of mass, momentum, and energy that can be written as follows:

Continuity
$$\frac{\partial u}{\partial x}+\frac{\partial v}{\partial y}=0 \tag{1}$$

x-momentum
$$u\frac{\partial u}{\partial x}+v\frac{\partial u}{\partial y}=-\frac{1}{\rho}\frac{\partial p}{\partial x}+\upsilon\left(\frac{\partial^2 u}{\partial x^2}+\frac{\partial^2 u}{\partial y^2}\right)+g\,\beta\sin\Phi(T-T_c) \tag{2}$$

y-momentum
$$u\frac{\partial v}{\partial x}+v\frac{\partial v}{\partial y}=-\frac{1}{\rho}\frac{\partial p}{\partial y}+\upsilon\left(\frac{\partial^2 v}{\partial x^2}+\frac{\partial^2 v}{\partial y^2}\right)+g\,\beta\cos\Phi(T-T_c) \tag{3}$$

Energy
$$u\frac{\partial T}{\partial x}+v\frac{\partial T}{\partial y}=\alpha\left(\frac{\partial^2 T}{\partial x^2}+\frac{\partial^2 T}{\partial y^2}\right)-\frac{1}{\rho c_p}\nabla.q_r \tag{4}$$

2.2. Gas Radiation Modeling

Since, the gas radiation effect is considered in the simulation, besides the convective and conductive terms, the radiative term is also present in the energy equation. In this equation, $\nabla.q_r$ can be calculated as [22]:

$$\nabla.q_r=\sigma_a\left(4\pi I_b(\vec{r})-\int_{4\pi} I(\vec{r},\vec{s})\,d\Omega\right) \tag{5}$$

where σ_a is the absorption coefficient, $I(\vec{r},\vec{s})$ is the radiation intensity at position r and in the direction s, and $I_b(\vec{r})=\sigma(T(\vec{r}))^4/\pi$ is the black body radiation intensity. To obtain the radiation intensity field and $\nabla.q_r$, it is

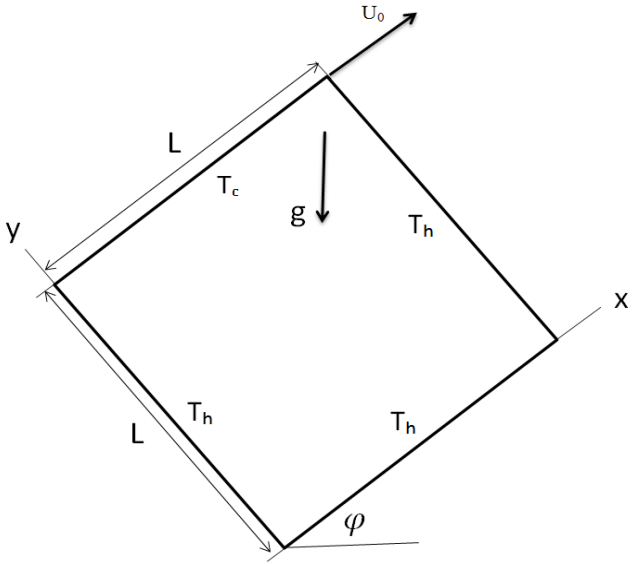

Fig.1. Schematic of computational domain

necessary to solve the radiative transfer equation (RTE). This equation for an absorbing, emitting and scattering gray medium can be written as [22]:

$$\begin{aligned} &\mathrm{s}.\nabla \mathrm{I}(\vec{\mathrm{r}},\vec{\mathrm{s}}) \\ &= \sigma_{\mathrm{a}}(\vec{\mathrm{r}})\mathrm{I}_{\mathrm{b}}(\vec{\mathrm{r}}) - \beta(\vec{\mathrm{r}})\mathrm{I}(\vec{\mathrm{r}},\vec{\mathrm{s}}) \\ &+ \frac{\sigma_{\mathrm{s}}(\vec{\mathrm{r}})}{4\pi}\int_{4\pi} \mathrm{I}\,(\vec{\mathrm{r}},\vec{\mathrm{s}'})\emptyset\big(\vec{\mathrm{r}},\vec{\mathrm{s}},\vec{\mathrm{s}'}\big)\mathrm{d}\Omega' \end{aligned} \tag{6}$$

In which σ_s is the scattering coefficient, $\beta = \sigma_s + \sigma_a$ is the extinction coefficient, and $\emptyset\big(\vec{r},\vec{s},\vec{s'}\big)$ is the scattering phase function for the radiation from incoming direction $s'$and confined within the solid angle $d\Omega'$ scattered toward direction s confined within the solid angle $d\Omega$. In this study, isotropic scattering medium is considered, in which the scattering phase function is equal to unity. The boundary condition for a diffusely emitting and reflecting gray wall is:

$$\begin{aligned} &I(\vec{r}_w,\vec{s}) = \\ &\varepsilon_w I_b(\vec{r}_w) + \tfrac{1-\varepsilon_w}{\pi}\int_{\vec{n}_w.\vec{s'}<0} I\,(\vec{r}_w,\vec{s})\big|\vec{n}_w\cdot \\ &\vec{s'}\big|d\Omega' \qquad \vec{n}_w\cdot\vec{s} > 0 \end{aligned} \tag{7}$$

where ε_w is the wall emissivity, $I_b\left(\vec{r}_w\right)$ is the black body radiation intensity at the temperature of the boundary surface, and n_w is the outward unit vector normal to the surface. For Eqs. (1) to (4), no-slip boundary condition is employed as the boundary condition for the momentum equations and for the energy equation, the fluid temperature at the solid surfaces are kept equal to the wall temperature which is considered as T_h and T_c on the hot and cold walls, respectively.

2.3. Radiative Transfer Equation

In this work, the RTE is solved by using the discrete ordinates method (DOM). In this method, the RTE is substituted by a set of M discrete equations for a finite number of directions Ω_m, and each integral is substituted by a quadrature series. By this technique, the radiative transfer equation becomes as follows:

$$\begin{aligned} &(\Omega_{\mathrm{m}}.\nabla)\mathrm{I}(\mathrm{r},\Omega_{\mathrm{m}}) \\ &= -\beta\mathrm{I}(\mathrm{r},\Omega_{\mathrm{m}}) + \sigma_{\mathrm{a}}\mathrm{I}_{\mathrm{b}}(\mathrm{r}) \\ &+ \frac{\sigma_{\mathrm{s}}}{4\pi}\sum_{\mathrm{k}=1}^{\mathrm{M}} \mathrm{w}_{\mathrm{k}}\,\mathrm{I}(\mathrm{r},\Omega_{\mathrm{k}})\emptyset\big(\Omega_{\mathrm{m}},\Omega_{\mathrm{k}}\big) \end{aligned} \tag{8}$$

subjects to the boundary condition:

$$\begin{aligned} &\mathrm{I}(\mathrm{r}_{\mathrm{w}},\Omega_{\mathrm{m}}) \\ &= \epsilon\mathrm{I}_{\mathrm{b}}(\mathrm{r}) \\ &+ \frac{(1-\varepsilon)}{\pi}\sum_{\mathrm{n}.,\Omega_{\mathrm{k}}<0} \mathrm{w}_{\mathrm{k}}\,\mathrm{I}(\mathrm{r}_{\mathrm{w}},\Omega_{\mathrm{k}})|\mathrm{n}.\Omega_{\mathrm{k}}| \end{aligned} \tag{9}$$

where w_k is the ordinate weight. This angular approximation transforms the original equation into a set of coupled differential equations. In Cartesian coordinates, Eq. (8) becomes:

$$\xi_{\mathrm{m}}\frac{\partial \mathrm{I}_{\mathrm{m}}}{\partial \mathrm{x}} + \eta_{\mathrm{m}}\frac{\partial \mathrm{I}_{\mathrm{m}}}{\partial \mathrm{y}} + \beta\mathrm{I}_{\mathrm{m}} = \beta\mathrm{S}_{\mathrm{m}} \tag{10}$$

where S_m is a shorthand for the radiative source function that can be calculated by the following equation:

$$\begin{aligned} &\mathrm{S}_{\mathrm{m}} \\ &= (1-\omega)\mathrm{I}_b(\mathrm{r}) \\ &+ \frac{\omega}{4\pi}\sum_{\mathrm{k}=1}^{\mathrm{M}} \mathrm{w}_{\mathrm{k}}\,\mathrm{I}(\mathrm{r},\Omega_{\mathrm{k}})\emptyset(\Omega_{\mathrm{m}},\Omega_{\mathrm{k}}) \end{aligned} \tag{11}$$

in which ω is the albedo coefficient, $\omega = \sigma_s/\beta$. By the finite volume method, the following equation can be obtained for computing the radiant intensity for central nodes at each control volume [22]:

$$\mathrm{I}_{\mathrm{pi}} = \frac{|\xi_{\mathrm{i}}|\mathrm{A}_{\mathrm{x}}\mathrm{I}_{\mathrm{xi}}\mathrm{i} + |\eta_{\mathrm{i}}|\mathrm{A}_{\mathrm{y}}\mathrm{I}_{\mathrm{yi}}\mathrm{i} + \mathrm{S}_{\mathrm{pi}}}{\beta\forall + |\xi_{\mathrm{i}}|\mathrm{A}_{\mathrm{x}} + |\eta_{\mathrm{i}}|\mathrm{A}_{\mathrm{y}}} \tag{12}$$

in which ξ_i, η_i are the directional cosines and $\forall$ is the element cell volume. For the radiative boundary conditions, the walls are assumed to emit and reflect diffusely with constant wall emissivity of ε_w=0.8.

2.4. Non-dimensional Forms of the Governing Equations

In the numerical solution of the set of governing equations including the continuity, momentum, and energy, the following nondimensional groups are used

$$\mathrm{X} = \frac{\mathrm{x}}{\mathrm{L}}, \qquad \mathrm{Y} = \frac{\mathrm{y}}{\mathrm{L}}, \qquad \mathrm{U} = \frac{\mathrm{u}}{\mathrm{U}_0},$$

$$\mathrm{V} = \frac{\mathrm{v}}{\mathrm{U}_0}, \qquad \mathrm{P} = \frac{\mathrm{p}}{\rho\mathrm{U}_0^2}, \qquad (1-\omega) = \frac{\sigma_{\mathrm{a}}}{\beta},$$

$$\tau = \beta\mathrm{L}, \qquad \mathrm{RC} = \frac{\sigma\mathrm{L}\mathrm{T}_{\mathrm{h}}^3}{\mathrm{k}}, \qquad \Theta = \frac{\mathrm{T}-\mathrm{T}_{\mathrm{c}}}{\mathrm{T}_{\mathrm{h}}-\mathrm{T}_{\mathrm{c}}},$$

$$\theta_1 = \frac{T_c}{T_h - T_c}, \qquad \theta_2 = \frac{T_h}{T_c}, \qquad I^* = \frac{I}{\sigma T_h^4},$$

$$S^* = \frac{S}{\sigma T_h^4}, \qquad q_r^* = \frac{q_r}{\sigma T_h^4}, \qquad Pe = Re.Pr,$$

$$Gr = \frac{g\beta(T_h - T_c)L^3}{\vartheta^2}, \qquad Re = \frac{\rho U_0 L}{\mu}$$

The governing equations for laminar steady two-dimensional mixed convection, after applying the Boussinesq approximation and neglecting the viscous dissipation, can be expressed in the dimensionless forms as follows:

$$\frac{\partial U}{\partial X} + \frac{\partial V}{\partial Y} = 0 \tag{13}$$

$$U\frac{\partial U}{\partial X} + V\frac{\partial U}{\partial Y} = -\frac{\partial P}{\partial X} + \frac{1}{Re}\left(\frac{\partial^2 U}{\partial X^2} + \frac{\partial^2 U}{\partial Y^2}\right) + \left(\frac{Gr}{Re^2}\Theta\right)\sin\Phi \tag{14}$$

$$U\frac{\partial V}{\partial X} + V\frac{\partial V}{\partial Y} = -\frac{\partial P}{\partial Y} + \frac{1}{Re}\left(\frac{\partial^2 V}{\partial X^2} + \frac{\partial^2 V}{\partial Y^2}\right) + \left(\frac{Gr}{Re^2}\Theta\right)\cos\Phi \tag{15}$$

$$U\frac{\partial \Theta}{\partial X} + V\frac{\partial \Theta}{\partial Y} = \frac{1}{Re.Pr}\left(\frac{\partial^2 \Theta}{\partial X^2} + \frac{\partial^2 \Theta}{\partial Y^2}\right) - \frac{\tau(1-\omega)RC\theta_1\theta_2}{Pe}\left[\frac{4}{\theta_2^4}\left(\frac{\Theta}{\theta_1} + 1\right)^4 - \sum_{k=1}^{M} I_k^* w_k\right] \tag{16}$$

The velocity and temperature boundary conditions have the following dimensionless forms:

at X=0 and X=1 U=V=0 and $\Theta = 1$

at Y=0 U=V=0 and $\Theta = 1$

at Y=1 U=1, V=0 and $\Theta = 0$

The values of convective, radiative, total and average Nusselt numbers at the walls can be calculated as follows:

$$Nu_c = \frac{q_c L}{k\Delta T} = -\frac{\partial \Theta}{\partial Y} \tag{17}$$

$$Nu_r = \frac{q_r L}{k\Delta T} = RC.\theta_1.\theta_2\, q_r^* \tag{18}$$

$$Nu_t = Nu_c + Nu_r \tag{19}$$

$$\overline{Nu} = \frac{1}{A}\int_A Nu\, dA \tag{20}$$

3. Method of Solution

Since the buoyancy term appears in the flow equations and also because the RTE depends on the temperature field through the emission term, all the governing equations should be solved simultaneously. The finite difference forms of the continuity, momentum and energy equations were obtained by integrating an elemental cell volume with staggered control volumes for the x- and y-velocity components. Other variables of interest were computed at the grid nodes. Discrete procedure utilizes the line-by-line method connected to the finite volumes technique with the Hybrid method [23] for calculating the fluxes at the faces of the control volumes and central differencing is used to discretize the diffusion terms. These computations are coded into a computer program in FORTRAN. Based on the result of the grid tests for obtaining the grid-independent solutions, six different meshes were used in the grid independence study. The corresponding maximum values of convective and total Nusselt numbers at the bottom wall of the lid-driven cavity are calculated and tabulated in Table 1. The grid-independence study was achieved with a uniform grid size of 60×60, while using a denser mesh of 80×80 resulted in less than 2.1% difference in the value of Nusselt numbers at the bottom wall. Therefore, the grid of 60×60 is sufficient for this simulation.

In this study, for computing the divergence of radiative heat flux by the DOM, S_4 approximation has been used. In computing radiant intensity, the numerical solution of Eq.(10) can be started with the black body assumption for the boundaries by neglecting the source term S_i. In the next iteration, the general forms of Eq.(12) and its boundary condition are applied. This procedure is repeated until the convergence criterion is met. Finally, from the radiative intensity obtained from Eq. (12), the divergence of radiative heat flux, which is needed for the numerical solution of the energy equation, can be calculated. The computation is terminated when the residuals for the continuity, momentum and energy equations get below 10^{-5}. By this numerical strategy, the velocity, temperature and radiation intensity distributions inside the flow domain can be obtained.

4. Code Validation

4.1. Validation of Convective Heat Transfer Results

The computational procedure is validated against the numerical results of Iwatsu et al. [24] for a top-heated moving lid with adiabatic side walls and bottom-cooled square cavity filled with air (Pr = 0.71). A 100×100 mesh is used and the computations are carried out for four different values of Re and Gr combinations. The comparisons of the average Nusselt number at the hot lid are listed in Table 2. The general agreement between the present computation and that of Iwatsu et al. [24] is seen to be very well with a maximum discrepancy of about 4%.

For another test case, validation was performed by comparing the streamlines and isotherm contours for an inclined cavity with $\phi = 30°$ between the present work and a study by Abu-Nada and Chamkha [16], while pure mixed convection flow takes place inside the enclosure. The comparison shows excellent agreement for both streamlines and isotherm contours as displayed in Figs. 2 and 3.

Table 1. Grid independence study, Ri=1, RC=10, $\omega = 0.5, \tau = 0.01$

Grid size	Value of the maximum convective Nusselt number	Value of the maximum total Nusselt number
30 × 30	1.050	6.677
40 × 40	1.052	6.795
50 × 50	1.053	6.877
60 × 60	1.054	6.933
70 × 70	1.054	6.972
80 × 80	1.054	7.000

Table 2. Comparison of the computed average Nusselt number at the hot wall

Re	Gr	Present	Iwatsu.et al. [24]	Diff.%
100	102	1.99	1.94	-2.5
400	102	3.93	3.84	-2.3
100	104	1.28	1.34	1.4
400	104	3.49	3.62	3.6

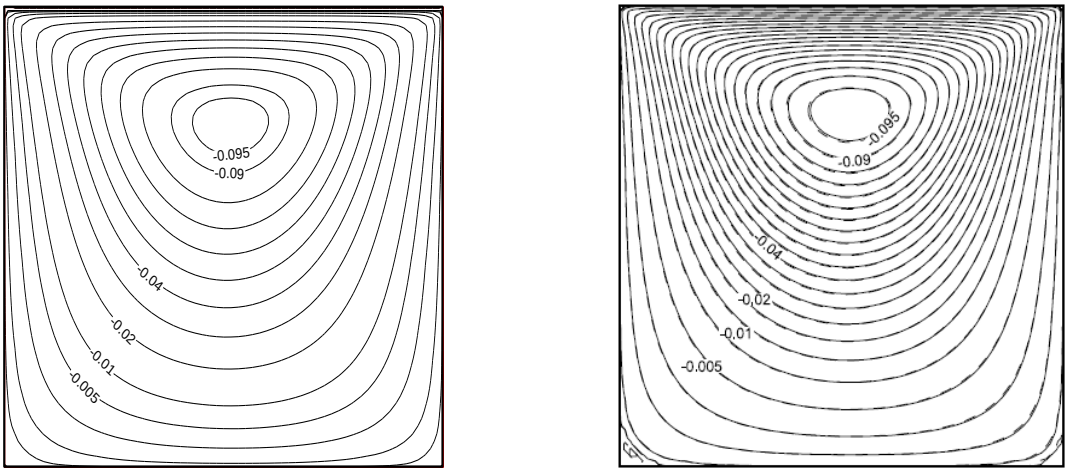

(a) : present study (b) : Abu-Nada and Chamkha [16]

Fig. 2. Distribution of the streamlines Re = 10, RI = 1, $\phi = 30°$

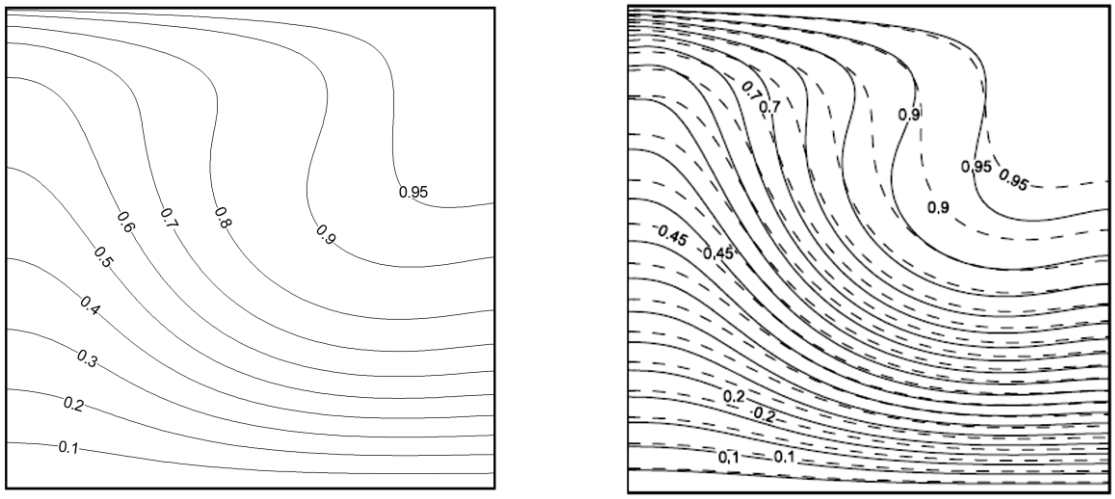

(a) : present study (b) : Abu-Nada and Chamkha [16]

Fig. 3. Distribution of the isotherm contours Re = 10, Ri= 1 and $\phi = 30°$

It should be noted that in Fig. 3-b, the isotherm drawn by a dash line is due to the temperature distribution in a nanofluid inside the cavity that was under study in Ref. [16] and is not of interest for the present work.

4.2. Validation of Combined Conductive-Radiative Heat Transfer Results

To check the performance and accuracy of the DOM and radiative computations, a test case is considered with a square enclosure of length L, containing an absorbing, emitting and scattering medium in which a combined conductive-radiative heat transfer takes place. The left wall of the enclosure is hot and other walls are cold, with the non-dimensional temperatures equal to 1 and 0.5, respectively. This problem was solved numerically by Mahapatra et al. [25] by using the DOM. The variation of temperature in the mid plane of enclosure along the horizontal axis is shown in Fig. 4 with a comparison to the result obtained by Mahapatra et al. [25]. As it is seen, a good agreement is achieved.

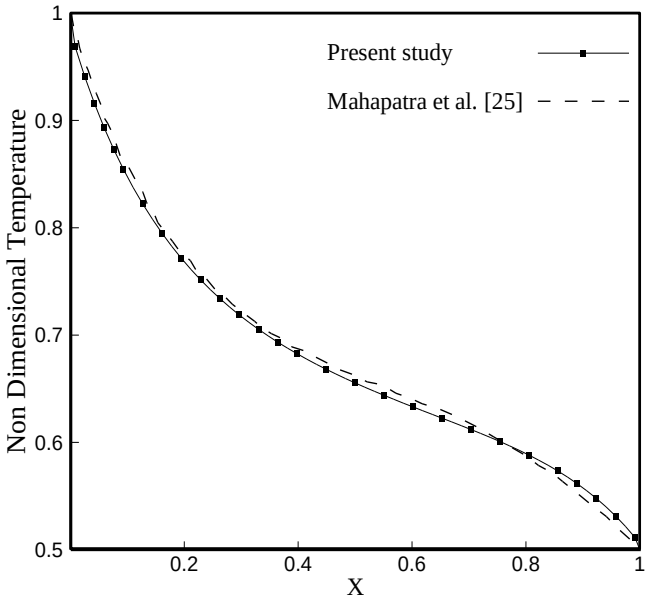

Fig. 4. Comparison of the computed mid-plane temperature with theoretical result by Mahapatra et al. [25]
RC = 10, $\omega = 0.5, \varepsilon_w = 0.1, \tau = 1$

Besides, in Fig. 5, the isotherm lines inside the enclosure obtained by the present computation are compared to those found in Ref. [25]. There is also a good consistency between these theoretical results.

5. Results and Discussions

This study presented the numerical results for a mixed convection laminar flow of a radiating gas in an inclined cavity at different radiant parameters, Richardson number and inclination angle. First, the impact of varying the Richardson number (Ri) on the flow field and temperature contours for various inclination angles is illustrated in Figs. 6, 7 and 8. The value of Richardson number shows the importance of the thermal natural convection forces relative to the forced convection effect due to an induced lid-driven effect. It should be mentioned that mixed convection flows with $\mathrm{Ri} \gg 1, \mathrm{Ri} \approx 1$ and $\mathrm{Ri} \ll 1$ pertain to natural convection dominance, mixed convection, and dominating forced convection, respectively. In the case of fluid flow in a cavity without an inclination angle (ϕ=0°), Fig. 6-a shows a very big recirculated domain inside the cavity that rotates in the clockwise direction, and also a small bubble that occurs near the right bottom corner. This figure depicts that the center of the main recirculated zone moves toward the direction of lid movement. One can notice the fact that in mixed convection flow inside a lid-driven cavity, there are two driving forces for generating fluid flow. One is the moving surface (forced convection effect) and the other is the buoyancy force (free convection). In the present test case with small value of Ri, the effect of forced convection is dominant. By considering this fact, it can be found that the flow pattern does not change considerably because of the cavity inclination. So that Fig. 6-b, which shows the streamlines for ϕ=30°, the distribution of streamlines is nearly close to that for ϕ=0°, and with this small change, two small bubbles are generated close to the bottom corners. For the cases with ϕ=60°and ϕ=90°, the same trend is seen, so that a main recirculated zone appears in nearly the whole domain of the cavity and small bubbles are formed close to the bottom corners.

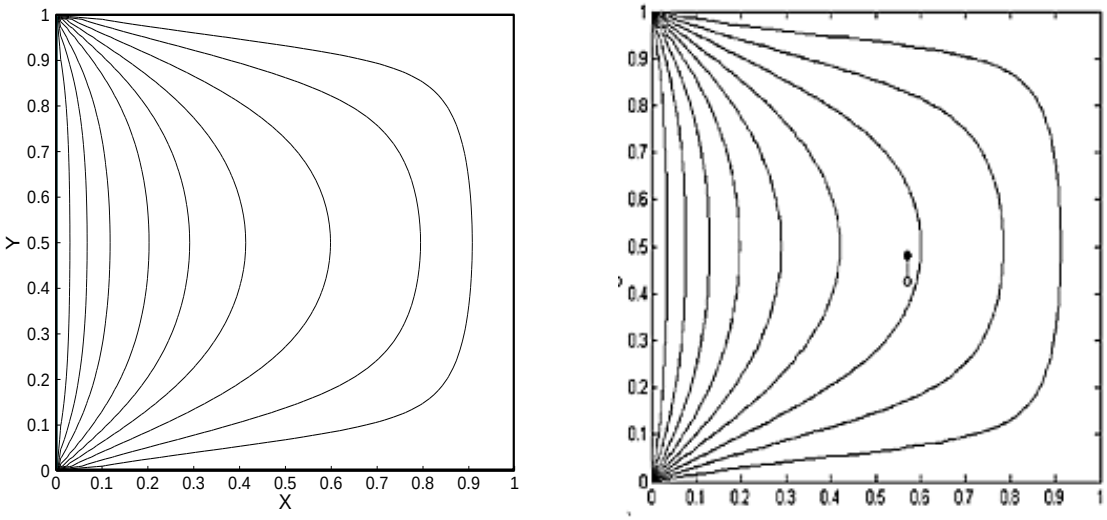

(a) Present study (b) Mahapatra et al. [25]

Fig. 5. Distribution of isotherm lines inside the cavity studied in Ref. [25]
RC = 10, $\boldsymbol{\omega = 0.5, \varepsilon_w = 0.5, \tau = 1}$

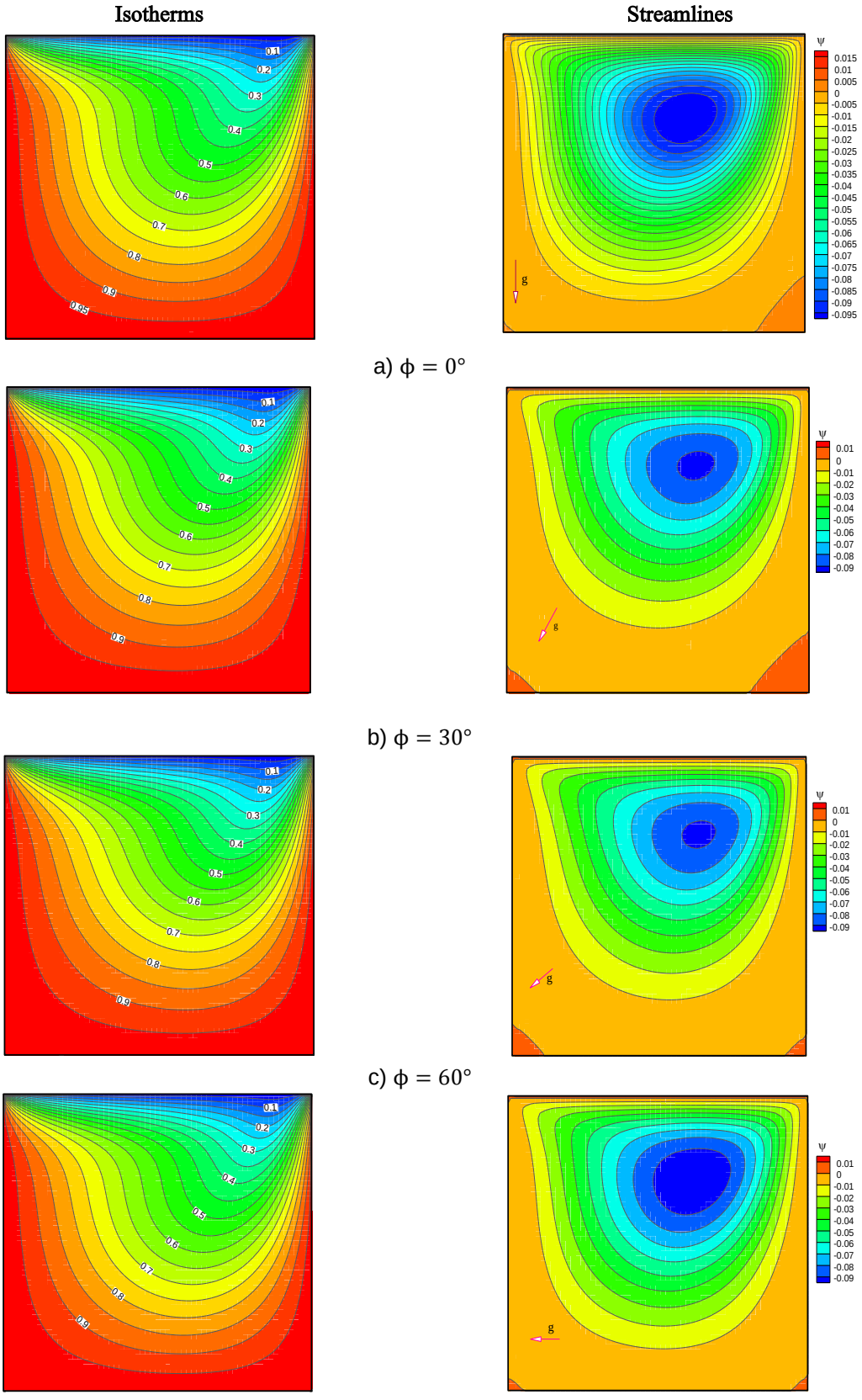

Fig. 6. Streamlines and temperature contours at different inclination angles for Ri = 0.1, RC = 10, ω = 0.5, τ = 0.01

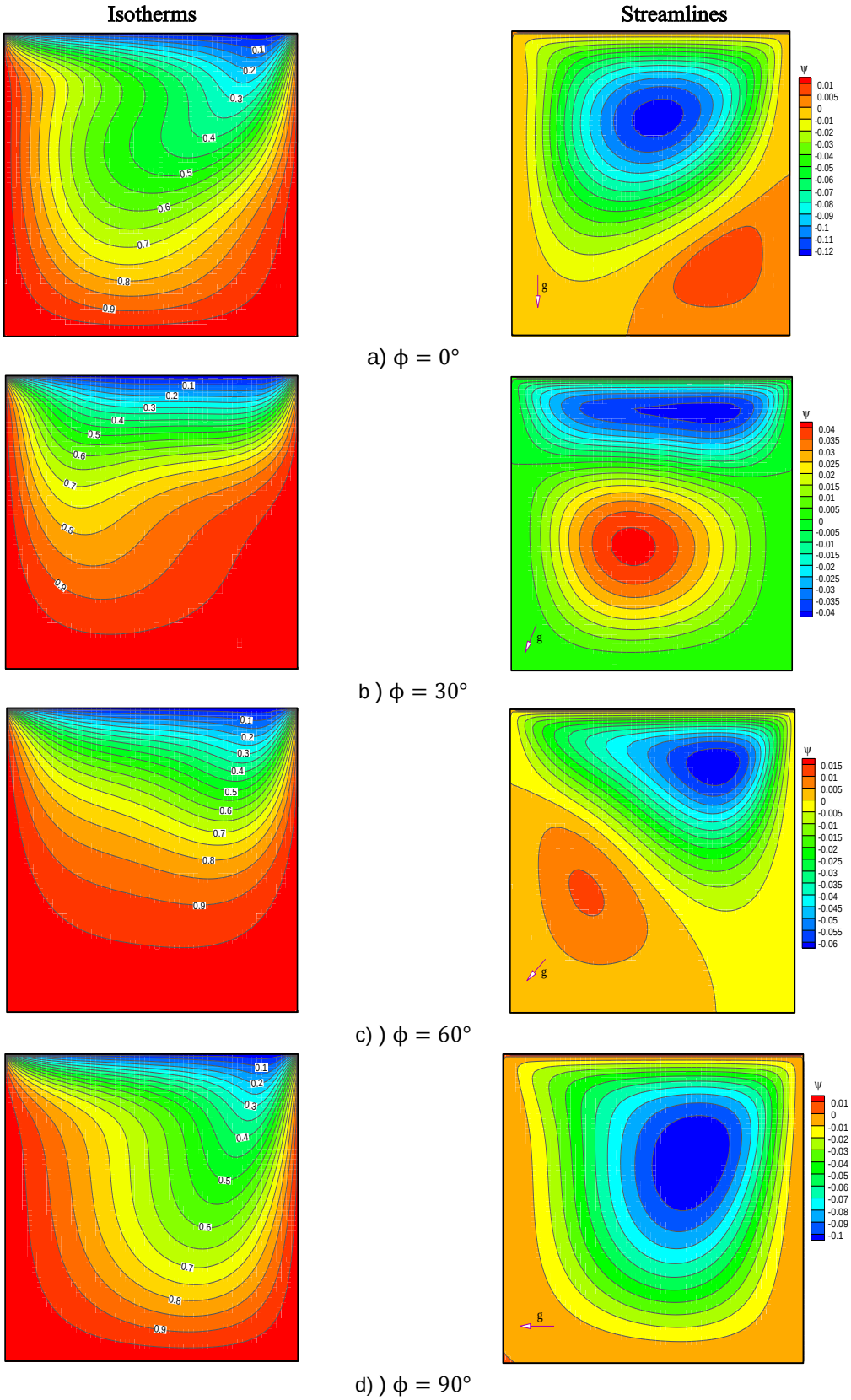

Fig. 7. Streamline and isotherm contours for Ri = 1, RC = 10, $\omega = 0.5, \tau = 0.01$

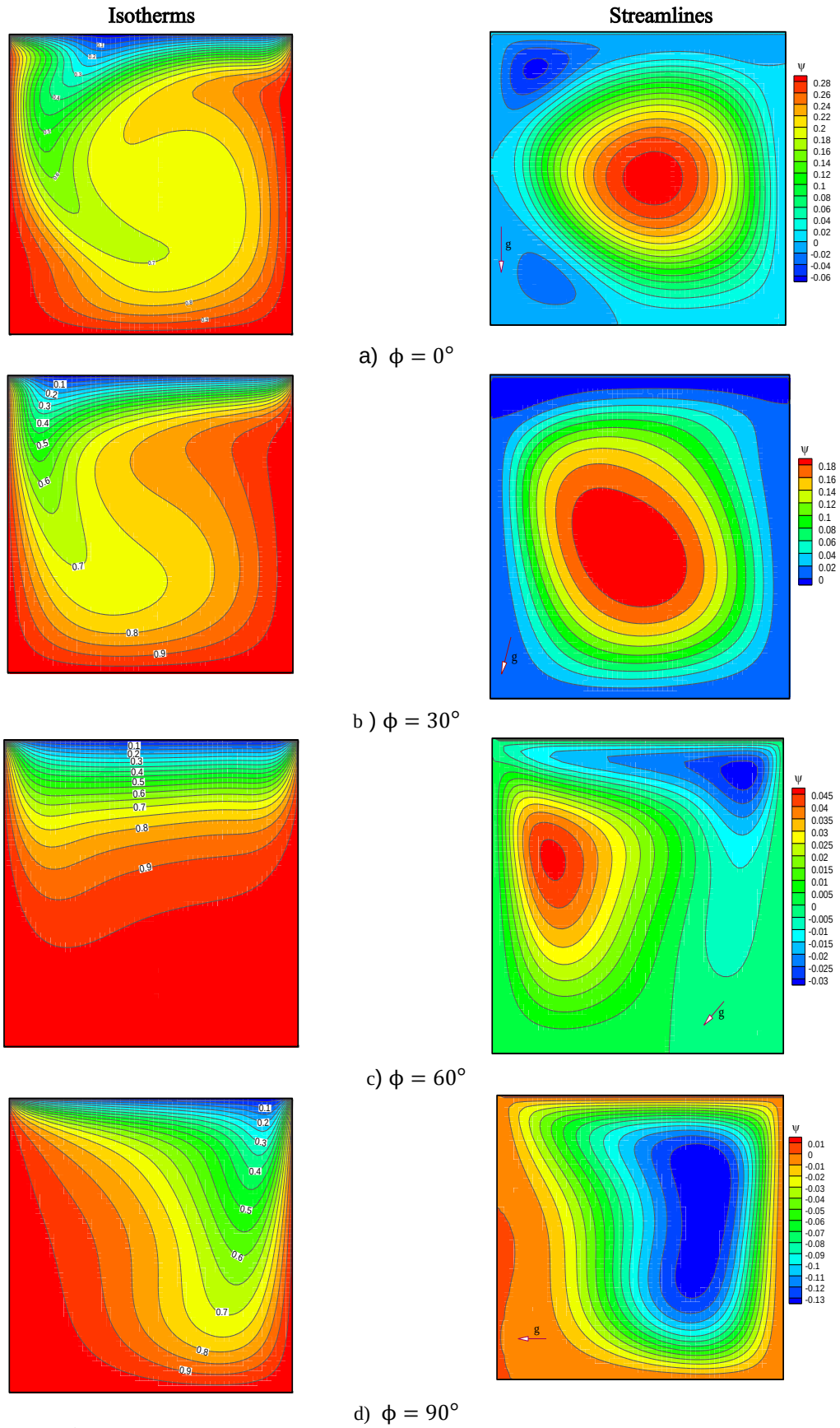

Fig. 8. Streamline and isotherm contours for Ri=10, RC=10, $\omega = 0.5, \tau = 0.01$

The temperature distributions inside the cavity flow at different values of inclination angle are also depicted in Fig. 6. It is seen that the temperature gradient near the top moving surface is greater than the other walls, and also near the walls because of constant surface temperature; isotherm becomes parallel to the surfaces. Besides, it is found that in the case of Ri=0.1, the temperature distribution is not affected considerably by changing the cavity inclination angle. Similar curves are plotted in Fig. 7 in which the value of the Richardson number is equal to 1. Under this condition, both forced and free convection effects are in the same order. For ϕ=0°, the streamlines plotted in Fig. 7-a show a big recirculated zone adjacent to the moving wall and a smaller one near the bottom right corner. But Fig. 7 demonstrates that the flow pattern changes considerably when the cavity becomes inclined. So that for ϕ=30°, the recirculated domain near the moving top wall becomes smaller than the other one adjacent to the bottom wall, and by increasing the value of ϕ, a reverse behavior is seen in Fig. 7-c. In the case of ϕ=90°, it is seen that only one recirculated zone appears inside the cavity. This behavior can be explained by the fact that by rotation of the cavity with ϕ=90°, the natural and forced convection forces have the same direction near the lid-driven that causes the generation of a big recirculated zone with high vortices that occupies the whole region of the cavity. Besides, Fig. 7 demonstrates that the distribution of isotherm lines is much affected by the inclination angle. One of the other results that can be found from Fig. 7, is that the inclination angle has a sweep effect on the flow pattern. This behavior can be seen if one compares the flow patterns in the cases of ϕ= 0°, 30°, 60°, and 90°.

In this study, the distributions of streamlines and isotherms are also plotted for high Richardson number, say, Ri=10. Comparison between this figure and Fig. 7 reveals that the fluid flow and thermal behavior of the system are much affected by the cavity's inclined angle. As noted earlier, this is due to the fact that for a high value of Richardson number, the effect of buoyancy force increases and it is evident that the inclination angle has considerable effect on this driving force. So that for specific values of ϕ, the force and free convection become opposite, forcing the fluid flow to have a small recirculated domain, and for some other inclination angle under which these those two driving forces have the same direction, high extent recirculated zones appear.

The next figures are about the variations of convective and radiative Nusselt numbers along the bottom wall of the cavity, at different values of the inclination angle, optical thickness, scattering albedo and radiation-conduction parameters. First, the effects of inclined angle ϕ on the variations of Nu_c and Nu_r are studied in Fig. 9. As it is seen that both Nu_c and Nu_r have their minimum values at the corners and their maximum values near the middle of the bottom wall. As depicted in Fig. 9-a, the inclined angle has considerable effect on the distribution of convective Nusselt number, particularly on the value of $Nu_{c\,max}$.

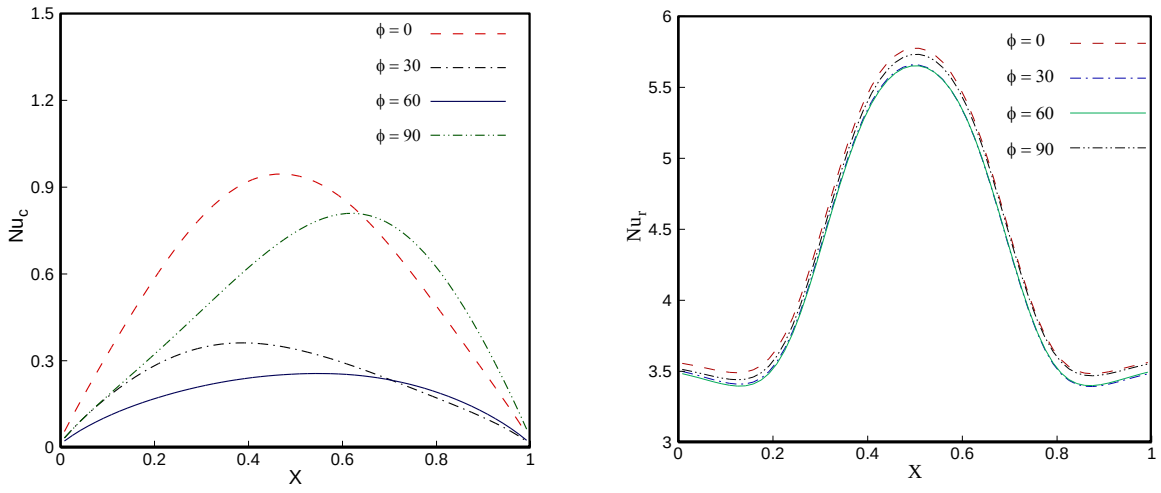

(a) Convective Nusselt number (b) Radiative Nusselt number

Fig. 9. Distributions of Nu_c and Nu_r along bottom surface of cavity at different inclination angle for Ri=1, RC=10, $\omega = 0.5, \tau = 0.1$

If one notices the curves plotted in Fig. 9(a), a sweep behavior is found on the variation of Nu_c, so that the maximum value of Nu_c first decreases with the increase of ϕ from 0° to 60°, and then it increases by further increase of ϕ up to 90°. As noted earlier, this behavior is due to the effect of inclined angle on the flow pattern and on the power of the vortices in the recirculated zone.

The distributions of radiative Nusselt number are also plotted in Fig. 9 at different values of ϕ. It is found that the inclination angle does not have considerable effect on Nu_r.

In Fig. 10, the distributions of Nusselt number along the bottom wall are plotted, but when the Richardson number has a high value equal to 10. As seen in Fig. 9 earlier, the same trend is also observed in this figure, but Fig. 10 reveals that the effect of inclined angle on Nu_c increases with increasing values of the Richardson number.

One of the important radiative parameters in a participating media is optical thickness, which shows the ability of the media to absorb and emit radiating energy. The effect of optical thickness on convective Nusselt number is demonstrated in Fig. 11(a). This figure shows an increasing trend for convective Nusselt number with increased optical thickness. This is due to the fact that in a participating media with high optical thickness, the radiation is strongly absorbed by the gas near the wall, thereby causing the media to have a high temperature gradient that leads to a high value for the convection coefficient.

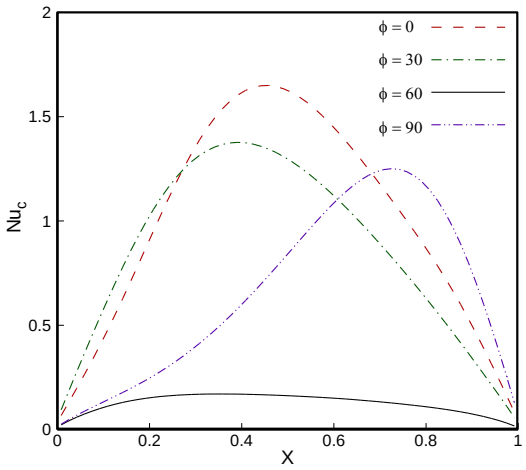

(a) Convective Nusselt number

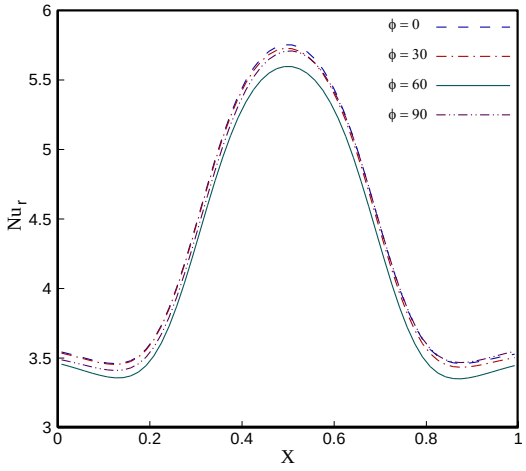

(b) Radiative Nusselt number

Fig. 10. Distributions of Nu_c and Nu_r along bottom surface of cavity at different inclination angle for Ri=10, RC=10, $\omega = 0.5, \tau = 0.1$

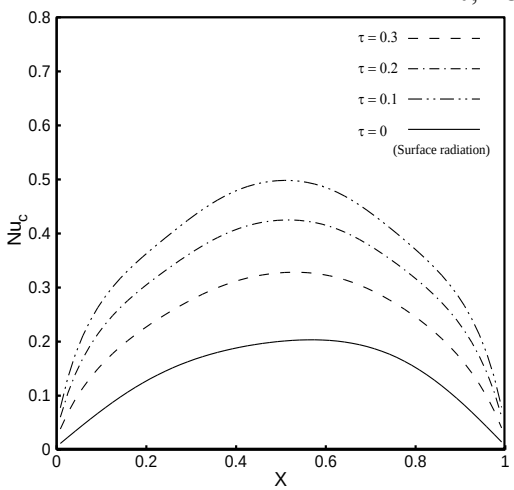

(a)Convective Nusselt number

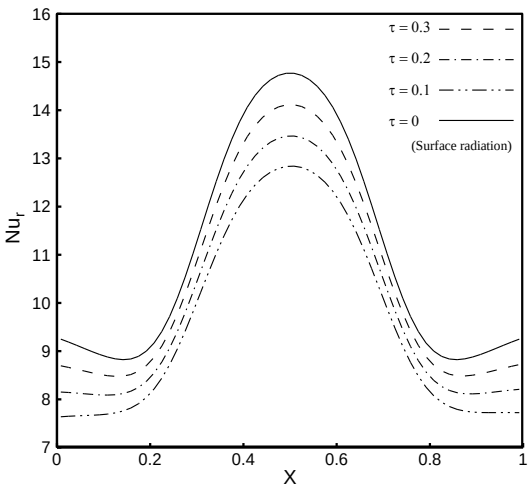

(b) Raditive Nusselt number

Fig. 11. Distributions of Nu_c and Nu_r along bottom surface of cavity at different optical thickness Ri=1, $\phi = 60°$, RC=25, $\omega = 0.5$

Figure 11(b) shows the effects of optical thickness on the distribution of Nu_r for four different values of optical thickness, including $\tau = 0$ that pertains to only surface radiation. It is seen that the values of Nu_r decreases by increasing τ. This is because of reduction in radiative heat flux at the hot wall due to increased gas absorption.

The effects of radiation-conduction parameter and also the effect of scattering on the distribution of total Nusselt number along the bottom wall of the cavity are presented in Figs. 12 and 13. As it is seen, increasing the RC parameter leads to an increase in the total Nusselt number and an opposite behavior is seen for Nu_t with variation of scattering albedo. But, it is seen that the RC parameter has more effect on the total Nusselt number in comparison to scattering albedo.

6. Conclusion

The present study numerically analyzed the mix convection flow of a radiating gas in a lid-driven cavity. Toward this end, the set of governing equations including the continuity, momentum and energy equations was solved by the CFD techniques. For computing the distribution of radiative heat flux inside the participating media, the RTE was solved numerically by the DOM. The results were presented by plotting the streamlines and isotherms inside the cavity and also by showing the distributions of the convective, radiative and total Nusselt numbers along the bottom wall. In this research work, an attempt was made to investigate the effect of cavity inclination angle on both the flow and thermal behaviors of the system. As a main result, it was revealed that the variation of inclination angle caused a sweep behavior in the flow pattern inside the cavity. Besides, the effects of several important parameters including the Richardson number, Radiation-Conduction parameter, optical thickness and scattering albedo on the variations of convective and radiative Nusselt numbers along the hot bottom wall were explored.

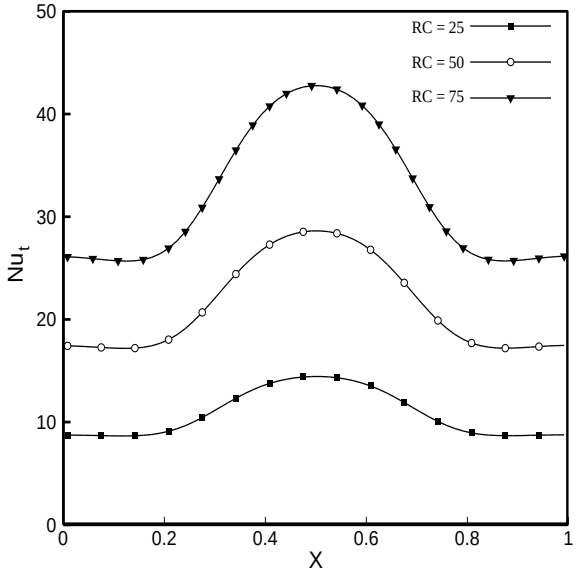

Fig. 12. Effect of RC on the total Nusselt number distribution along the bottom wall
Ri=1, $\phi = 60°, \tau = 0.1, \omega = 0.5$

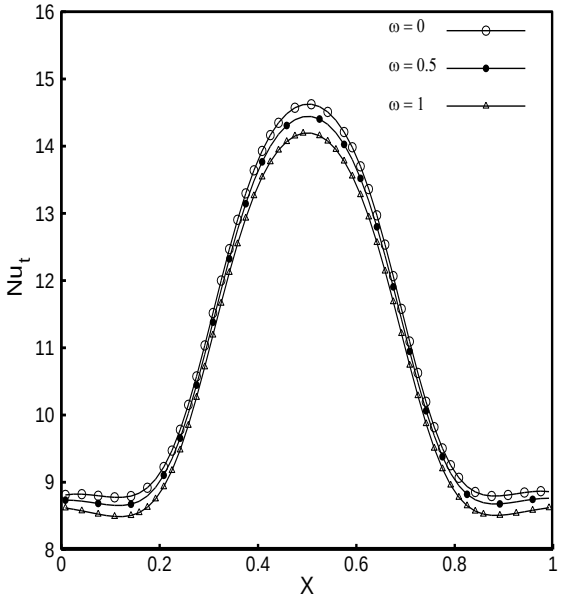

Fig. 13. Effect of albedo coefficient on the total Nusselt number distribution along the bottom wall
Ri=1,$\phi = 60°$, RC = 25, $\tau = 0.1$

References

[1] Burggraf O. R., Analytical and Numerical Studies of the Structure of Steady Separated Flows, Journal of Fluid Mechcanics (1996) 24(1):113–115.

[2] Ghia U., Ghia K. N., Shin C. T., High-Re Solutions for Incompressible Flow Using the Navier–Stokes Equations and a Multigrid Method, Journal of Computational Physics (1982) 48(3): 387–411.

[3] Pilkington L. A. B., Review Lecture:The Float Glass Process, Proceedings of Royal Society of London, Series A (1969) 314 (1516): 1-25, 1969.

[4] Ideriah F. J. K., Prediction of Turbulent Cavity Flow Driven by Buoyancy and Shear, Journal of Mechanical Engineering Science (1980) 22(6): 287–295.

[5] Imberger J., Hamblin P. F., Dynamics of Lakes, Reservoirs and Cooling Ponds, Annual Review of Fluid Mechcanics (1982) 14: 153–187.

[6] Cha C. K., Jaluria Y., Recirculating Mixed Convection Flow for Energy Extraction, International Journal Heat and Mass Transfer (1984) 27(10): 1801–1810.

[7] Prasad A. K., Koseff J. R., Combined Forced and Natural Convection Heat Transfer in a Deep Lid-Driven Cavity Flow, International Journal of Heat and Fluid Flow (1996) 17: 460–467.

[8] Leong J. C., Brown N. M., Lai F. C., Mixed Convection from an Open Cavity in a Horizontal Channel, International Communications in Heat and Mass Transfer (2005) 32: 583-592.

[9] Moallemi M. K., Jang K. S., Prandtl Number Effects on Laminar Mixed Convection Heat Transfer in a Lid-Driven Cavity, International Journal of Heat Mass Transfer (1992) 35(8): 1881–1892.

[10] Oztop H. F., Salema K. A., Pop I., MHD Mixed Convection in a Lid-Driven Cavity with Corner Heater, International Journal of Heat and Mass Transfer (2011) 54: 3494-3504.

[11] Sharif M. A. R., Laminar Mixed Convection in Shallow Inclined Driven Cavities with Hot Moving Lid on Top and Cooled from Bottom, Applied Thermal Engineering (2007) 27(5): 1036-1042.

[12] Alinia M., Ganji D. D., Gorji-Bandpy M., Numerical Study of Mixed Convection in an Inclined Two Sided Lid Driven Cavity Filled with Nano Fluid Using Two-Phase Mixture Model, International Communications in Heat and Mass Transfer (2011) 38 (10): 1428-1435.

[13] Oztop H. F., Natural Convection in Partially Cooled and Inclined Porous Rectangular Enclosures, International Journal of Thermal Sciences (2007) 46:149–156.

[14] Sivasankaran S., Sivakumar V., Hussein A. K., Numerical Study on Mixed Convection in an Inclined Lid-Driven Cavity with Discrete Heating, International Communications in Heat and Mass Transfer (2013) 46:112-125.

[15] Mohammad A. A., Viskanta R., Flow Structures and Heat Transfer in a Lid-driven Cavity Filled with Liquid Gallium and Heated from below, Experimental Thermal and Fluid Science (1994) 9(3): 309–319.

[16] Abu-Nada E., Chamkha A.J., Mixed Convection Flow in a Lid-Driven Inclined Square Enclosure Filled with a Nanofluid, European Journal of Mechanics B/Fluids (2010) 29(6): 472-482.

[17] Cheng T. S., Liu W.-H., Effects of Cavity Inclination on Mixed Convection Heat Transfer in Lid-Driven Cavity Flows, Computers & Fluids (2014) 100: 108-122.

[18] Prasad Y. S., Das M. K., Hopf Bifurcation in Mixed Convection Flow Inside a Rectangular Cavity, International Journal of Heat and Mass Transfer (2007) 50(17): 3583–3598.

[19] Sameh E. Ahmeda, Mansourb M.A., Mahdy A., MHD Mixed Convection in an Inclined Lid-Driven Cavity with Opposing Thermal Buoyancy Force: Effect of Non-uniform Heating on Both Side Walls, Nuclear Engineering and Design 265 (2013) 938– 948.

[20] Tan Z., Howell J. R., Combined Radiation and Natural Convection in a two Dimensional Participating Square Medium, International Journal of Heat and Mass Transfer (1991) 34: 785–793.

[21] Han C. Y., Baek S. W., The Effects of Radiation on Natural Convection in a Rectangular Enclosure Divided by Two Partitions, Numerical Heat Transfer, Part A (2000) 37: 249-270.

[22] Modest M. F., Radiative Heat Transfer, Academic Press, San Diego, Chapter 16 (2003).

[23] Patankar S. V., Spalding D. B., A Calculation Procedure for Heat, Mass and

Momentum Transfer in Three-Dimensional Parabolic Flows. International Journal of Heat and Mass Transfer (1972) 15(10): 1787–1806.

[24]Iwatsu R., Hyun J.M., Kuwahara K., Mixed Convection in a Driven Cavity with a Stable Vertical Temperature Gradient, International Journal of Heat and Mass Transfer (1993) 36 (6): 1601–1608.

[25]Mahapatra S. K., Dandapat B. K., A. Sarkar, Analysis of Combined Conduction and Radiation Heat Transfer in Presence of Participating Medium by the Development of Hybrid Method, Journal of Quantitative Spectroscopy & Radiative Transfer (2006) 102(2): 277–292.